Published in final edited form as:

Immunity. 2014 September 18; 41(3): 440–450. doi:10.1016/j.immuni.2014.07.013.

S1P-Dependent Trafficking of Intracellular *Yersinia pestis* through Lymph Nodes Establishes Buboes and Systemic Infection

Ashley L. St. John[1,2,*], **W.X. Gladys Ang**[3], **Min-Nung Huang**[4], **Christian A. Kunder**[2], **Elizabeth W. Chan**[4], **Michael D. Gunn**[4,5], and **Soman N. Abraham**[1,2,3,4]

[1]Program in Emerging Infectious Diseases, Duke-National University of Singapore, Singapore 169857, Singapore

[2]Department of Pathology, Duke University Medical Center, Durham, NC 27710, USA

[3]Department of Molecular Genetics and Microbiology, Duke University Medical Center, Durham, NC 27710, USA

[4]Department of Immunology, Duke University Medical Center, Durham, NC 27710, USA

[5]Department of Medicine, Duke University Medical Center, Durham, NC 27710, USA

SUMMARY

Pathologically swollen lymph nodes (LNs), or buboes, characterize *Yersinia pestis* infection, yet how they form and function is unknown. We report that colonization of the draining LN (dLN) occurred due to trafficking of infected dendritic cells and monocytes in temporally distinct waves in response to redundant chemotactic signals, including through CCR7, CCR2, and sphingosine-1-phospate (S1P) receptors. Retention of multiple subsets of phagocytes within peripheral LNs using the S1P receptor agonist FTY720 or $S1P_1$-specific agonist SEW2871 increased survival, reduced colonization of downstream LNs, and limited progression to transmission-associated septicemic or pneumonic disease states. Conditional deletion of $S1P_1$ in mononuclear phagocytes abolished node-to-node trafficking of infected cells. Thus, *Y. pestis*-orchestrated LN remodeling promoted its dissemination via host cells through the lymphatic system but can be blocked by prevention of leukocyte egress from DLNs. These findings define a novel trafficking route of mononuclear phagocytes and identify S1P as a therapeutic target during infection.

*Correspondence: ashley.st.john@duke-nus.edu.sg.

SUPPLEMENTAL INFORMATION

Supplemental Information includes six figures and Supplemental Experimental Procedures and can be found with this article online at http://dx.doi.org/10.1016/j.immuni.2014.07.013.

AUTHOR CONTRIBUTIONS

Experiments were predominately designed by A.L.S. and S.N.A. and performed predominately by A.L.S. and W.X.G.A. W.X.G.A. and M.D.G. contributed to experimental design and C.K., M.-N.H., and E.W.C. performed additional experiments. The manuscript was written by A.L.S. All authors contributed to discussions.

INTRODUCTION

Yersinia pestis is a Gram-negative bacterial pathogen that is responsible for more human deaths, historically, than any other infectious agent. As such, it constitutes a remarkable example where the mammalian immune system profoundly fails to contain infection within the host or subsequent spread within a population. After deposition of infectious bacteria subcutaneously by fleas, the most common route of exposure (Hinnebusch, 2005), disease is characterized by the formation of buboes, lymph nodes (LNs) that are swollen far beyond the degree that occurs with LN hypertrophy during the initiation of productive immunity (Butler, 1994; Perry and Fetherston, 1997). The virulence of *Y. pestis* has always been assumed to be dependent on the ability of this pathogen to enter the draining LNs (dLNs); however, little is known about the mechanisms of bubo formation or the utility of these pathological structures to the progression of disease systemically (Perry and Fetherston, 1997). Uncontained infection frequently progresses rapidly from bubonic plague, where the dLN is the predominate organ affected, beyond the initial site of infection to systemic forms affecting the blood (septicemic plague) or the lungs (pneumonic plague). Both of these more clinically serious disease states are associated with further bacterial spread to new hosts (Jawetz and Meyer, 1944; Perry and Fetherston, 1997). It is unknown, however, what route the bacteria take to establish systemic infection. In particular, the role played by the progressive development of buboes in the host is not understood, as is whether these structures are functional effectors of disease or merely evidence of disease as the host attempts to mount a protective adaptive immune response within LNs in the presence of considerable pathogen burden. Several notable bacterial pathogens are lymphotrophic, including *Salmonella* Typhimurium, which is closely related to *Y. pestis*, and others (Bar-Haim et al., 2008; St John and Abraham, 2009), but little of the mechanistic utility of targeting lymphoid tissue has been experimentally investigated.

We began these studies with the aim of elucidating the underlying basis of bubo formation and its contributions to *Y. pestis* virulence and in vivo trafficking in order to reveal in greater detail how the LN microenvironment responds to a substantial bacterial challenge. Our findings show that *Y. pestis* infects cell types including dendritic cells (DCs) and mononuclear phagocytes and exploits the trafficking routes of these cells to achieve systemic infection. Transit of *Y. pestis*-infected cells between LNs via the lymphatic system was shown to be dependent on Sphingosine-1-phosphate (S1P). These results demonstrate the importance of mononuclear phagocytes to the pathogenesis of bubonic plague and define a new trafficking route for monocytic cells that can occur during infection.

RESULTS

Infected Cellular Compartments of LNs during *Y. pestis* Infection

To begin our investigation of the mechanism of bubo formation, we infected mice with *Y. pestis* subcutaneously in their rear footpads to replicate the natural route of infection prior to the infiltration of the dLN. The footpad also has the advantage of being drained by a single sentinel LN, the popliteal node. We injected 1×10^5 CFU of *Y. pestis* Kim5 (hereafter referred to only as *Y. pestis*), a strain that retains all of its virulence factors but lacks the ‘‘pigmentation locus,’’ which facilitates iron acquisition (Brubaker et al., 1965; Perry et al.,

1990). As a result, these bacteria have slower growth in vivo than wild-type *Y. pestis*, allowing the initial stages of disease progression to be studied temporally. To begin, we sought to recapitulate within our model the characteristic dLN pathology that is observed clinically (Butler, 1994). During *E. coli* infection, which, in contrast, is quickly cleared in mice, dLNs swelled in size with the retention of greater numbers of lymphocytes from the circulation, so that at 24 hr post infection the dLNs may have doubled in size (Figure 1A; McLachlan et al., 2003). In contrast, *Y. pestis*-infected dLNs surpassed the size of dLNs responding to *E. coli* infection and displayed a characteristic pathology with swollen sinuses, or sinus histiocytosis (Figure 1A). Similar to reports of clinical infection and models of infection with WT *Y. pestis* (McLachlan et al., 2003; Sebbane et al., 2005), mice had progressive bubo formation, characterized by necrotic lesions that were visible beginning around 24 hr after infection, based on staining of sections with propidium iodide (Figure S1 available online). The areas of necrosis progressively grew, often constituting large regions of the DLN by 72 hr after infection (Figure S1). Careful examination of swollen dLN sinuses 24 hr after *Y. pestis* infection revealed that they are full of cellular infiltrates that are histologically consistent with macrophages (Figure 1B). We also observed by transmission electron microscopy (TEM) that many of these cells contained individual or multiple bacteria within vesicular compartments (Figure 1C), consistent with previous findings that macrophages can be infected and that viable *Y. pestis* is frequently found intracellularly in vivo (Cavanaugh and Randall, 1959; Finegold, 1969; Janssen and Surgalla, 1969; Marketon et al., 2005; Straley and Harmon, 1984). These observations indicate that *Y. pestis*-induced buboes contain massive infiltrates of macrophages, many of them harboring intracellular bacteria.

Multiple phagocytic cell types can be infected by *Y. pestis*, including macrophages and DCs (Cavanaugh and Randall, 1959; Saikh et al., 2004; Zhang et al., 2008). After observing intracellular bacteria within dLNs by TEM (Figure 1C), we investigated the phenotype of the infected cells in order to determine which cellular compartments were infected within dLNs over a time course of bubo formation. We expressed orange fluorescent protein (YP-OFP) in *Y. pestis* (YP-OFP), which allowed us to subject single-cell suspensions of dLNs to surface staining for cellular markers, followed by flow cytometry to define the populations containing intracellular bacteria. We also verified that OFP expression did not alter the kinetics of bacterial spread in vivo (data not shown). At 6 hr after injection of bacteria into the footpads, more than 90% the infected cells within the dLN were predominately double positive (DP) for CD11c and CD11b (Figure 2A). At the same time, bacteria were not detected inside $CD11b^{+}CD11c^{-}$ cells (Figure 2A), which correspond broadly to a non-DC monocyte or macrophage cell type (Geissmann et al., 2003). By 24 hr after infection, YP-OFP could be detected inside these $CD11b^{+}$ single-positive (SP) cells, and the percentage of $CD11b^{+}$ SP infected cells gradually increased over the course of the next days, becoming approximately equivalent in numbers to the percentage of infected cells that were $CD11c^{+}CD11\ b^{+}$ DCs by around 48 hr after infection, and surpassing them to become the predominately infected cell type by 72 hr (Figure 2A). The percentage of infected cells was also consistent with the trend for total numbers of infected cells in the dLN, which increased the most over the initial 24 hr of infection (Figure S2A). To further define the cell types that were infected phenotypically, we performed flow cytometry after staining using a full panel

of myeloid cell markers. At 24 hr after infection, intracellular *Y. pestis* were detected within LN DCs ($CD11c^+IA/IE^+$) as well as neutrophils (PMN, $Ly6G^{hi}$) and, to a lesser extent, inflammatory monocytes (iMono; $CD11b^+LY6C^+F4/80^+IA/IE^-$) (Figure 2B). We further defined the infected DC populations and observed that most infected DCs were $CD11b^+$, with much smaller populations of $CD11b^-$ DCs and monocyte-derived DCs (moDC; $CD11c^+CD11b^+IA/IE^+Ly6C^+$) also containing intracellular *Y. pestis* (Figure 2C). Examining total cells, we observed substantial infiltration of iMono, moDCs, and neutrophils compared to resting conditions (Figure 2D). To further support that intracellular OFP-expressing *Y. pestis* were contained within myeloid cells, we conjugated these bacteria to magnetic particles prior to infection of footpads, using an established protocol (Lönnbro et al., 2008). At 24 hr after infection, LNs were harvested and prepared as single-cell suspensions. When the bacteria within the preparations were magnetically isolated, intracellular bacteria were recovered that were contained within cells staining positive for myeloid markers (Figure S2B). By confocal microscopy, we could visualize the colocalization of OFP with CD11b and/or CD11c within sectioned and stained LN tissue (Figures 2E and S5). Bacteria were seen inside cells expressing CD11c and CD11b at the 24 hr time point (Figures 2E and S4). Consistent with our flow cytometry data, at 72 hr, OFP colocalized primarily with $CD11b^+$ cells, but colocalization with CD11c staining was often not detectable (Figures 2E and S5). Cumulatively, these flow cytometry and fluorescent microscopy results suggest that there are two distinct waves of infection within dLNs, the first primarily of DCs, which are known to migrate from sites of peripheral inflammation to the dLN early after cutaneous infection (Shelburne et al., 2009), and the second of non-DC myeloid cells, likely to be monocytes, macrophages, and neutrophils.

Directed Migration of DCs and Monocytes Enhances dLN Infection

Features of *Y. pestis* infection are the progression of dLN pathology beyond the normal extent of LN hypertrophy that is induced during similar infections (Figure 1A) and the transition of the cellularity of the LN structure to a profile characterized by the marked increase of $CD11b^+$ non-DC cell types within dLNs, which is significant by 24 hr after infection (Figure 2A). We hypothesized that there might be changes in chemokine expression within dLNs that could promote the mass influx of macrophages that is observed during *Y. pestis* infection. Therefore, we harvested dLNs from mice infected as described above and isolated RNA to determine the expression of several chemokines that are able to recruit multiple subsets of monocytes and macrophages (Charo and Ransohoff, 2006; Proudfoot, 2002). By real-time PCR, we determined substantial increases in the expression of chemokines, including CCL2, CCL3, CCL4, and CXCL10 (also known as MCP-1, MIP-1α, MIP-1β, and IP-10, respectively) within dLNs with *Y. pestis* infection, compared to saline controls (Figures 2F and S6). Each of these chemokines has a well-established role in the recruitment of monocytes, DCs, and/or macrophages (Cross et al., 1997; Shi and Pamer, 2011). In order to compare *Y. pestis*-induced chemokine increases within the context of other infections, we also examined the chemokine production in LNs to two other Gram-negative pathogens, *Escherichia coli* (where infection remains confined to the site of infection) and *Salmonella* Typhimurium (which has well-established dLN-targeting adaptations) (St John and Abraham, 2009). These additional bacterial pathogens also induced subtle increases in the expression of chemokines within dLNs over saline injection;

however, the increases were far below the drastic changes in chemokine expression evoked by *Y. pestis* (Figure 2F). Thus, an overabundance of monocyte and macrophage chemoattractants in dLNs characterizes *Y. pestis* infection, resulting in the arrival of a broad panel of cells permissive to infection or already-infected cells from the site of infection.

Based on the observations that large numbers of infected cells within dLNs are migratory phagocytes and that chemoattractants for these cells are broadly upregulated in the first 24 hr of infection, we aimed to directly test the contributions of cellular trafficking to containment or enhancement of *Y. pestis* infection. CCR2-deficient mice were chosen since this chemokine receptor has been shown to direct chemotaxis into sites of inflammation, toward CCL2 (Geissmann et al., 2003; Lin et al., 2008), which is one of the chemokines that is expressed more abundantly in *Y. pestis*-infected dLNs than other infections we examined (Figure 2F). In mice infected with *Y. pestis*, we observed that a subset of inflammatory monocytes (which have been identified by others based on their CCR2-directed migration [Geissmann et al., 2003; Lin et al., 2008]) were reduced in numbers in the dLNs of *Ccr2*$^{-/-}$ mice compared to WT mice, where recruitment into the dLN of cells expressing both F4/80 and CD11b was impaired (Figure S3). However, a population of cells expressing CD11b alone still infiltrated, although they appeared to be largely confined to the dLN sinuses (Figure S3). Next, we quantified the numbers of bacteria within dLNs at 24 hr in *Ccr2*$^{-/-}$ and WT mice to determine whether CCR2 could influence the numbers of bacteria in the dLN. Mice were infected in their footpads, as above, and dLNs were harvested after 24 hr. Although the absence of this chemokine receptor did not entirely abolish intracellular bacteria within dLNs, we found that *Ccr2*$^{-/-}$ mice had significantly reduced numbers of *Y. pestis*-infected cells in their dLNs compared to WT mice (Figure 3A). Thus, the infiltration of inflammatory monocytes into the dLN contributes to the ability of *Y. pestis* to replicate within or spread to the dLN.

CCR2 is only one of many chemokine receptors having the potential to direct monocyte migration to the dLNs, but the first cells to be infected there appeared to be DCs (Figures 2A, 2C, and 2D), which largely migrate very early after activation (within hours of peripheral *E. coli* infection) (Shelburne et al., 2009) and in response to a constitutive chemotactic gradient of CCL21 (Randolph et al., 2005). Therefore, we also investigated whether mice lacking the receptor for CCL21, CCR7, had fewer bacteria within DLNs during *Y. pestis* infection. Although a caveat of use of these mice is that they have additional alterations to LN morphology, including compartmentalization of T cells, they have greatly reduced LN-homing capacity of DCs (Förster et al., 1999). Notably, the background strains of CCR7-deficient and CCR2-deficient mice vary in these experiments (BALB/c and C57BL/6, respectively), which is known to influence the kinetics and tolerance of *Y. pestis* infection in mice (Turner et al., 2008). Therefore, we optimized the dose of *Y. pestis* required for lethal infection and *Ccr7*$^{-/-}$ mice and BALB/c controls were administered a larger inoculating dose of 1×10^7 CFU in footpads. In *Ccr7*$^{-/-}$ mice, similarly to *Ccr2*$^{-/-}$ mice, intracellular *Y. pestis* were reduced in dLNs by 24 hr, compared to controls, as determined by flow cytometry (Figure 3B). We also observed that localized pretreatment of wild-type mice (C57BL/6) with a neutralizing antibody against CCL21 within the footpad substantially reduced the increased CCL2 expression that was observed in LNs at 24 hr after

infection compared to administration of an isotype control antibody (Figure 3C). As expected, CCL21 neutralization also decreased the number of $CD11c^+$ DCs within *Y. pestis*-infected LNs at 24 hr (Figure 3D) and the CFU of *Y. pestis* in the dLN at 24 hr (Figure 3E), emphasizing the role of early DC trafficking in both bacterial invasion of dLNs and in prompting the subsequent chemokine production and resulting enhanced phagocyte recruitment.

We anticipated that, as a result of significantly reduced bacterial burden within dLNs 24 hr after infection, *Ccr2*$^{-/-}$ or *Ccr7*$^{-/-}$animals could have improved infection outcomes compared to their wild-type controls. Therefore, we examined the spread of bacteria to organs that are targets during systemic infection, such as the lungs and the spleen, and survival during lethal challenge. For *Ccr2*$^{-/-}$ mice there appeared to be a trend toward reduced bacterial spread to systemic infection, since the mean CFUs in the spleen and lungs 3 days after subcutaneous infection seemed to be reduced; however, these reductions were not statistically significant (Figure 3F). The mice did have modestly but significantly prolonged survival after lethal challenge (Figure 3G), suggesting that CCR2-directed migration of inflammatory monocytes is a contributing factor to *Y. pestis* pathogenesis in vivo. In contrast, reductions in bacterial spread to both the spleen and lungs in vivo after subcutaneous infection in *Ccr7*$^{-/-}$ mice were statistically significant compared to wild-type (Figure 3H). Importantly, *Ccr7*$^{-/-}$ mice had a significant survival advantage and 60% of these mice recovered from this otherwise lethal challenge (Figure 3I). The ability to use these two individual mouse tools to promote survival emphasizes that trafficking of multiple cellular subsets of phagocytic cells are involved in the in vivo pathogenesis of *Y. pestis*. Since blocking each chemokine-dependent trafficking route independently resulted in significantly reduced dLN colonization (Figures 3A, 3B, and 3E) but for *Ccr2*$^{-/-}$ mice did not result in statistically significant reductions in the numbers of bacteria colonizing distal target organs under these experimental conditions (Figure 3F), it seemed that multiple and/or redundant chemotactic pathways had an additive effect in carrying the bacilli to LNs and distal organs. Therefore, we began to investigate the events that allow distribution of *Y. pestis* beyond the sentinel bubo and the role of cellular trafficking in this event.

Intracellular Dissemination of *Y. pestis* through the Lymphatic Vasculature

Because dLNs are highly vascularized, the bacilli might target this organ to promote direct inoculation of the blood in LNs, particularly since *Y. pestis*-infected LNs experience substantial necrosis beginning in the early days of infection (Figure S1). Despite the presence of growing necrotic lesions within massively swollen LNs, the high endothelial venules in LNs appeared intact in tissue sections and did not show any signs of the vasculature having lost its barrier function to the blood (Figure S4). At 72 hr, numerous colonies of bacteria could be grown from homogenates of the spleen and lungs of WT mice (Figures 3F and 3H), signaling that a systemic infection had already been established. Our alternate hypothesis is that phagocytes not only facilitate the movement of bacteria into dLNs, but that, once there, phagocytes also disseminate bacteria beyond the dLN to downstream LNs, by traveling through lymphatics. The structure of the mammalian lymphatic vasculature is such that lymph passes through sentinel dLNs and exits via the efferent lymph. It then drains (along with any cellular constituents) to higher-order LNs until

finally this fluid is restored to circulation by the thoracic duct. Cells morphologically consistent with both DCs and macrophages have been isolated from the efferent lymph in the thoracic duct (Anderson et al., 1981; Bell, 1979; De Martini et al., 1983), raising the possibility that these recirculating cells could be a direct route into the bloodstream for intracellular bacteria. To determine whether intracellular bacteria could be found inside cells in transit between LNs, we performed confocal microscopy. After injection of OFP^+ *Y. pestis* into footpads, animals were perfused with paraformaldehyde to preserve antigenic integrity and the rear legs decalcified to promote sectioning through the thigh tissue. Tissue sections were then stained for CD11b (expressed by most infected cells in dLNs, Figure 2A) and Lyve-1^+ lymphatics. OFP^+ bacilli could be viewed intracellularly in $CD11b^+$ cells within the postnodal lymphatics that depart the popliteal LN (Figure 4A). This suggests that intracellular transport of *Y. pestis* between LNs did occur. Furthermore, we verified the presence of intracellular bacteria within the second-order iliac node by performing a gentamicin protection assay. The iliac node was processed to produce a single-cell suspension followed by treatment with gentamicin to kill extracellular bacteria, only including any that might be adherent to the surface of cells. The CFUs of intracellular bacteria within the iliac LN were then determined. When compared to the total numbers of bacteria in the iliac LN, it became apparent that at 24 hr, more than 80% of *Y. pestis* in the iliac LN are intracellular, a ratio that decreased over time after LN colonization (Figure 4B), although total intracellular numbers continued to increase until 48 hr and subsequently declined (Figure 4C). This suggests the role of the intracellular population in early sequential LN colonization.

S1P Receptor Targeting to Limit Bacterial Spread In Vivo

Since our data using $Ccr7^{-/-}$ or $Ccr2^{-/-}$ mice revealed that deficiency for each chemokine receptor, individually, could not substantially prevent establishment of systemic *Y. pestis* infection, we looked for another mechanism to impair trafficking to test the hypothesis that *Y. pestis* reaches distant organs via intracellular travel through the lymphatic system. For DCs, travel between LNs is thought to be dependent on S1P signaling, with unique S1P receptors providing differential contributions to the regulated egress of independent DC subsets from LNs (Rathinasamy et al., 2010); however, less is known about the regulated exit of non-DC monocytes from LNs, or whether this occurs. We verified that the S1P receptor 1 ($S1P_1$) was highly expressed on both DP and SP populations of CD11b and CD11c stained cells in LNs and footpads and found that even for $CD11b^+CD11c^-$ cells, ~98% of these cells also expressed $S1P_1$ (Figures S5A and S5B). Based on this, we employed the broadly acting S1P receptor agonist, FTY720 (also known as Fingolimod), which binds multiple S1P receptors to block cellular exit from LNs (Brinkmann et al., 2002; Rivera et al., 2008). Prior to use, we verified that FTY720 did not have any direct bactericidal or bacteriostatic affect on *Y. pestis* by performing studies of growth kinetics in vitro (data not shown). FTY720 also did not increase the numbers of apoptotic cells in dLNs compared to vehicle alone (Figures S5C and S5D). Mice were pretreated with FTY720 24 hr prior to subcutaneous infection with *Y. pestis* and, subsequent to infection, were treated daily. Since the iliac LNs are higher-order nodes, which obtain efferent lymph that has passed through the popliteal node, we examined these LNs for evidence of altered *Y. pestis* trafficking during FTY720 administration. After 24 hr, in FTY720-treated mice, total

numbers of cells were reduced compared to vehicle controls at baseline for all single-or double-positive populations of CD11b/CD11c-stained cells in both popliteal (Figure 5A) and iliac (Figure 5B) nodes. Similarly, numbers of infected phagocytes, defined as OFP^+, were substantially reduced in the popliteal (Figure 5C) and iliac (Figure 5D) LNs for FTY720-treated mice, compared to mice administered the drug vehicle. As expected based on the results in Figure 2A, only a very small minority of infected cells were CD11c SP (data not shown). This trend that FTY720 reduced total cellularity of $CD11b^+$ and $CD11c^+$ cells was continued at 48 hr (Figure S5E). We also performed a CFSE-labeling experiment to track travel of infected cells from the site of instillation and through LNs. For this, CFSE was injected into footpads prior to infection with *Y. pestis* and flow cytometry was performed from single-cell suspensions of LNs after 24 hr to quantify the numbers of YP-OFP^+ and $CFSE^+$ cells in the LNs of FTY720-treated animals, compared to vehicle-treated animals. These results revealed that just as FTY720 treatment can act to reduce many subsets of infected and uninfected cells within primary and secondary order LNs (Figures 5A–5D), the accumulation in LNs of footpad-derived infected cells, which are presumably a key founder population in sequential LN colonization, is also substantially blocked (Figures 5E and 5F). Background levels of travel of CFSE-labeled cells were not detected within LNs outside of the context of infection (data not shown). Interestingly, with infection, CFSE-labeled cells made their way to iliac nodes, signifying that within 24 hr, infected cells can transit completely through the dLN (Figure 5F).

Because FTY720 is best described for its effective inhibition of T cell recirculation through lymphoid organs (Matloubian et al., 2004), we also verified that the observed effect of FTY720 in reducing infected DCs and monocytes within dLNs was not dependent on T cells. T cell depletion by antibody was chosen as a strategy over the use of nude mice since the latter lack T cells but also have described morphological defects within LNs (Sainte-Marie and Peng, 1983). After successful depletion of >98% of T cells (data not shown), followed by FTY720 treatment and infection, FTY720 still effectively reduced the numbers of CD11b SP and $CD11c^+CD11b^+$ cells within popliteal (Figure 5G) and iliac (Figure 5H) LNs in the absence of T cells. Additionally, when bacterial burden was assessed in the lungs and the spleens of infected mice 3 days after infection, we observed that FTY720 also dramatically reduced the numbers of bacteria in these organs (Figure 5I). To support a role for S1P receptors in the dissemination of *Y. pestis*-infected cells in vivo, we used a second compound, SEW2871, which is considered to be a specific agonist of $S1P_1$ (Rivera et al., 2008). Treatment of animals with SEW2871 resulted in reduced numbers of infected cells in the iliac but not popliteal LNs, implicating $S1P_1$ specifically in the travel of infected cells *between* LNs, but not in the initial event of dLN colonization (Figures 5J and 5K). Similarly, pretreatment of footpads with CFSE to label cells demonstrated that this generalized observation can be extended to those cells that were footpad resident and that became infected with YP-OFP, where SEW2871 did not reduce the total numbers of OFP^+CFSE^+ within the popliteal LN, but did reduce the total numbers in iliac LNs, compared to vehicle controls (Figures 5L and 5M). This suggests that other S1P receptors can compensate for inhibition of $S1P_1$ during the initial colonization of the dLN during $S1P_1$-specific blockade. For example, most infected DCs in the footpad and dLN expressed $S1P_3$ (Figures S5E–S5G). Since our data pertaining to FTY720 and SEW2871 focused on examining the

influence of these drugs on the trafficking patterns of infected cells, we also confirmed that consistent results were obtained in terms of total CFU in LNs. In agreement with data for infected cell populations, FTY720 significantly reduced *Y. pestis* CFU in both popliteal (Figure 5N) and iliac (Figure 5O) LNs, while SEW2871 did not influence CFUs in popliteal LNs (Figure 5N), but significantly reduced CFUs in iliac LNs (Figure 5O). In support of the importance of node-to-node travel in the establishment of systemic infection, both FTY720 and SEW2871 (Figure 5P) treatment promoted survival of challenged mice. Therefore, blocking the intranodal trafficking of infected cells by targeting the S1P pathway offers substantial protection from *Y. pestis*.

$S1P_1$ on Mononuclear Phagocytes Permits *Y. pestis* Exit from dLNs

To corroborate the drug studies that we performed and further interrogate the role of $S1P_1$ in intranodal trafficking by *Y. pestis*-infected mononuclear phagocytes, we generated conditional gene-deletion mice with $S1P_1$ deleted in CX3CR1-expressing cells. The mouse strain with CX3CR1-driven cre expression was chosen since this chemokine receptor is broadly expressed within the monuclear phagocyte system (Yona et al., 2013). These mice were bred to mice with the $S1P_1$ locus flanked by loxP sites. We first validated that there was efficient functional deletion resulting in loss of surface expression of $S1P_1$ on $CX3CR1^+$ cells, specifically, by performing flow cytometry to assess the expression of $S1P_1$ on $CX3CR1^+$ cells compared to $CX3CR1^-$ cells as an internal control. Mice carrying the floxed allele (*Cx3cr1*-Cre $S1pr1^{fl/fl}$) showed efficient deletion, whereas littermate control mice (*Cx3cr1*-Cre $S1pr1^{+/+}$) had expression of $S1P_1$ on $CX3CR1^+$ cells (Figure 6A). No alterations in the cellularity of LNs were observed at the steady state in *Cx3cr1* -Cre $S1pr1^{fl/fl}$ compared to *Cx3cr1* -Cre $S1pr1^{+/+}$ controls (Figure S6). We observed that 24 hr after infection with *Y. pestis*, numbers of intracellular bacteria were substantially decreased in secondary iliac LNs in *Cx3cr1* -Cre $S1pr1^{fl/fl}$ mice compared to *Cx3cr1*-Cre $S1pr1^{+/+}$ controls (Figure 6B). Similar to our prior observations that other S1P receptors can compensate for any utilization of $S1P_1$ by infected cells for travel to DLNs (Figure 5), we did not observe a significant reduction in the numbers of *Y. pestis*-containing cells in the primary popliteal LN at 24 hr after infection (Figure 6B). In support of the importance of $S1P_1$ on mononuclear phagocytes to *Y. pestis* dissemination through the lymphatic system, we observed that *Y. pestis*-infected *Cx3cr1*-Cre $S1pr1^{fl/fl}$ mice had significantly reduced mortality compared to *Cx3cr1*-Cre $S1pr1^{+/+}$ controls after subcutaneous inoculation of bacteria (Figure 6C). Our results show that $S1P_1$ expression is important for trafficking of *Y. pestis*-infected cells from primary to secondary LNs after peripheral infection and that this process of dissemination has consequences for survival.

DISCUSSION

These studies expose the role of the lymphatic system as a conduit for virulent pathogens to achieve systemic infection and reveal the underlying mechanism behind bubo formation during *Y. pestis* infection to be dependent on the chemotaxis of multiple subsets of DCs and monocytes. Furthermore, we show that *Y. pestis* is able to capitalize on the host's chemotactic pathways to travel to and within lymphoid tissue, first, by exploiting cellular trafficking of DCs to colonize dLNs as an intracellular, founder population and then by

promoting cellular trafficking of additional DCs and inflammatory monocytes into LNs. This occurs based on the upregulation of a broad panel of chemokines, including CCL2 and others, and use of the S1P receptors to travel to dLNs. Our results also emphasize the importance of the $S1P_1$ receptor, specifically, for guiding infected mononuclear phagocytes between the primary draining LN and secondary LNs. Conditional gene-deleted mice that lack the $S1P_1$ receptor on $CX3CR1^+$ cells, which are myeloid lineage mononuclear phagocytes (Yona et al., 2013), have significantly diminished spread of intracellular *Y. pestis* to the second order LNs in our model, the iliac nodes, while the numbers of bacteria in the popliteal, or primary dLN, are not significantly influenced. $S1P_1$-mediated dissemination of *Y. pestis* reduces survival during infection since CX3CR1-Cre $S1P_1^{fl/fl}$ mice are more resistant to *Y. pestis*-associated death than littermate controls.

CCL21 promotes the initial egress of DCs to the LNs from sites of infection and is required for subsequent upregulation of monocyte chemoattractants within LNs. CCL21 blockade also significantly reduces the number of bacteria in the dLN in the first 24 hr of infection, emphasizing the adverse functional consequences of the *travel* of DCs in promoting the initial colonization of LNs with *Y. pestis*. This suggests that the original migrating DCs from the site of infection containing intracellular bacteria play an important role in establishing infection in the dLN. We also observe that there is significantly decreased bacterial spread to the lungs and spleen and increased survival of mice lacking CCR7, further emphasizing this key DC chemotactic pathway involving CCL21 and CCR7 in *Y. pestis* pathogenesis. Once cells are infected peripherally, cellular trafficking into the dLN as a second site of infection is further augmented by increased chemokine production within dLNs. Our results also suggest that this process is promoted by S1P receptors since FTY720 treatment can dramatically reduce the numbers of infected cells in dLNs. In addition to the possibility that monocyte chemoattractants could promote subsequent colonizations by peripherally infected cells, they may, alternatively, promote the arrival of uninfected cells in LNs that could be infected by those bacteria that are already there, allowing additional in situ intracellular replication of *Y. pestis*. There is a shift in the cell type that is predominantly infected beginning around 48 hr after infection, so that most infected cells are non-DC cell types, expressing the marker CD11b, which are primarily monocytes and neutrophils that have phagocytosed bacteria. Monocytes have long been recognized to be able to be infected by *Y. pestis* and here we demonstrate, through the use of CCR2-deficient mice, that their recruitment is also consequential to disease progression, promoting bubo formation and hastening death. We note, however, that a caveat to use of $Ccr2^{-/-}$ mice is the complication that they also have reduced monocyte egress from the bone marrow (Tsou et al., 2007). Although the effects of chemokine receptor deficiency are significant, they are also modest in comparison to S1P blockade, presumably since multiple inflammatory cytokines with monocyte- or macrophage-recruiting functions are induced that may serve a redundant function. The proinflammatory factors produced by inflammatory monocytes may also amplify the recruitment of additional DCs and monocytes through the site of infection and to dLNs. The possibility exists that other defects in these knockout mice, such as altered efflux of cells from the bone marrow or entry into the tissue site likely contribute to the phenotypes observed and this is an important caveat to ascribing function to a unique chemotactic response in distributing *Y. pestis* systemically. Interestingly, for additional bacterial

infections, including *Listeria monocytogenes*, *Brucella melitensis*, and *Mycobacterium tuberculosis*, CCR2-mediated recruitment of cells serves a protective role for the host (Shi and Pamer, 2011), while in other infectious contexts, including viral and parasitic infections, CCR2-mediated recruitment has been associated with pathology at the site of infection (Shi and Pamer, 2011). We observe that the strong upregulation of monocyte chemoattractants during *Y. pestis* infection within LNs drastically contrasts with the transcriptional programs that occur during infections by other Gram-negative bacteria. This is a site where infection and inflammatory responses directed at the tissue have hardly been inspected. Buboes have primarily been examined in the terminal stages of infection when they are already structures defined by overt pathology that is distinguishable from resting or even inflamed dLNs in terms of size, cellularity, and tissue viability (Sebbane et al., 2006a, 2006b). Our results suggest that bubo formation is a process that begins in the earliest hours of infection and one that is integral to the virulence of *Y. pestis*, allowing the quick progression of bacteria from a site of subcutaneous injection to systemic infection, which would be more conducive to host-to-host transmission.

Since, here, we have used a strain of *Y. pestis* that should have a reduced growth rate in peripheral tissues where iron is low, these processes may be hastened during the pathogenesis of wild-type *Y. pestis*. Due to its reduced virulence in vivo by peripheral routes, the Kim5 strain has not previously been used as a model of bubonic plague, although other groups have also reported that it can be lethal to mice after peripheral inoculation (Perry and Fetherston, 1997; Une and Brubaker, 1984). In spite of the accepted observation that mice are more resistant to Kim5 or other strains lacking the pigmentation locus than WT *Y. pestis* strains, this strain may be useful for studying the immunological responses to *Y. pestis* since it also provokes bubo formation and allows host survival for several days even at lethal doses.

Blocking of cellular egress from LNs with FTY720, or with similar drugs targeting the S1P pathway, is a highly promising therapy that has been employed successfully experimentally in additional contexts of inflammation such as to limit autoimmune conditions (Takabe et al., 2008). In these contexts, the functional effects are assumed to predominately be based on the role of S1P agonists in blocking the regulated departure of lymphocytes from LNs (Rosen and Goetzl, 2005; Takabe et al., 2008), although our data suggest that the actions of S1P agonists in reducing *Y. pestis* in vivo are not attributable to the described role of these drugs on T cells (Matloubian et al., 2004). With S1P agonist treatment, we see that multiple subsets of monocytic cells can also be targeted for retention in peripheral LNs. In the case of *Y. pestis* infection, FTY720 can be used to slow the advance of the disease from the tissue to dLN, from dLNs to higher-order LNs that collect lymph from multiple sentinel LNs, as well as to the more readily transmitted septicemic or pneumonic forms of infection. This suggests that passive dissemination of extracellular bacteria by lymph flow, as has been alluded to as a possible mechanism of bacterial spread based on the presence of extracellular *Y. pestis* within organs (Pujol and Bliska, 2005), is not as important in this infection as the route of intracellular trafficking. Like others, we have also observed that many *Y. pestis* are found extracellularly in buboes (Sebbane et al., 2005); however, this extracellular population becomes more abundant after LN colonization, following an initial phase where the

intracellular population is dominant. Unique S1P receptors govern independent phases of the transition from peripheral to systemic infection since the $S1P_1$-specific agonist, SEW2871, does not influence the number of bacteria that are able to invade to the dLN, but still reduces node-to-node travel of intracellular *Y. pestis*. In support, we observe that mice with a conditional knockout of $S1P_1$ in CX3CR1-expressing cells have reduced spread of bacteria to secondary LNs. This is consistent with the observations of others that DC travel to dLNs is dependent on differential S1P receptors depending on the tissue or origin and DC subset. However, in contrast to our findings, those studies using sterile inflammatory stimuli also suggested that travel of tissue-resident DCs to dLNs was primarily dependent on $S1P_1$ (Gollmann et al., 2008; Lamana et al., 2011; Rathinasamy et al., 2010). This raises the possibility that the nature of inflammatory stimulus may also influence the capacity of DCs or other subsets of phagocytic cells to home to dLNs in a manner dependent on individual S1P receptors. We also observed that $S1P_1$ deficiency on $CX3CR1^+$ cells did not appear to significantly influence LN cellularity in the resting state, further emphasizing the importance of the inflammatory context to cellular trafficking. We expect that slowing the spread of intracellular hijacking bacteria could not only alter the disease outcome for an individual, but could potentially limit disease progression within a host population since colonization of target organs such the lungs is associated with virulent bacterial spread. This application of S1P agonists may be of utility in targeting additional intracellular or lymphotrophic pathogens.

EXPERIMENTAL PROCEDURES

Mice

Six-week-old female C57BL/6 were purchased from the National Cancer Institute Animal Production Area. *Ccr2*$^{-/-}$ mice (C57BL/6 background) and *Ccr7*$^{-/-}$ mice (BALB/c background) were maintained in the Duke University Vivarium. All animals were housed at the Duke University Vivarium and protocols were approved by the Duke University Institutional Animal Care and Use Committee.

Bacterial Cultures and Infections

Cultures of *S. typhimurium* SL1344 and *E. coli* J96 were grown overnight in LB (Difco Laboratories) at 37°C. Cultures of *Y. pestis* Kim5 were grown 48–72 hr in brain heart infusion (BHI) broth (Fluka Analytical), under shaking conditions at room temperature. To generate strains of fluorescent *Y. pestis* Kim5, bacteria were transfected by electroporesis with plasmid containing the OFP gene and an antibiotic marker, followed by selection of colonies on antibiotic (Ampicillin) plates. For footpad injections, 1×10^5 CFU (C57BL/6 background) or 1×10^7 CFU (BALB/c background) of bacteria were injected in a 20 μl volume of sterile PBS. To determine CFUs in organs, infected mice were euthanized at the noted time points after infection and organs were harvested and the mass recorded. Tissues were then homogenized in sterile water using ceramic beads for 2 cycles of 60 s each using an automatic homogenizer. Homogenates were plated on BHI plates and the colonies were counted after 48–72 hr incubation at room temperature in order to calculate the CFU of whole organs or relative to the biopsy mass. For survival curves, infected animals were monitored every 12 hr for death or humane endpoints.

Fingolimod Preparation and Treatment

Fingolimod (also known as FTY720) or SEW2817 (both from Cayman Chemicals) were dissolved to 25 mg/ml in DMSO for storage at −80°C and diluted in sterile 2% hydroxypropyl-β-cyclodextrin (w/v) in PBS for injections. Mice were given 5 mg/kg of FTY720 or SEW2817 or an equivalent amount of vehicle i.p. starting 12 hr before infection and then every 24 hr after infection.

Statistical Analysis

Significance was determined by unpaired two-tailed Student's t tests to assess data where only two groups existed, or by one- or two-way ANOVA, as appropriate. The Dunnett post test was used to acquire p values when treatments were compared to the control alone. Significance for Kaplan-Meier Curves was determined by the log-rank test and Fisher's exact test was used to evaluate significance in the surviving proportions. Statistics were performed using Excel and Prism software.

Supplementary Material

Refer to Web version on PubMed Central for supplementary material.

ACKNOWLEDGMENTS

We would like to thank W. Zhang for providing antibody 2C11 for T cell depletion experiments and A.P.S. Rathore for critical manuscript review. The authors' work is supported by NIH grants R01 AI35678, R01 DK077159, R01 AI50021, R37 DK50814, and R21 AI056101.

REFERENCES

Anderson AO, Warren JT, Gasser DL. Presence of lymphoid dendritic cells in thoracic duct lymph from Lewis rats. Transplant. Proc. 1981; 13:1460–1468. [PubMed: 6972645]

Bar-Haim E, Gat O, Markel G, Cohen H, Shafferman A, Velan B. Interrelationship between dendritic cell trafficking and *Francisella tularensis* dissemination following airway infection. PLoS Pathog. 2008; 4:e1000211. [PubMed: 19023422]

Bell EB. Antigen-laden cells in thoracic duct lymph. Implications for adoptive transfer experiments. Immunology. 1979; 38:797–808. [PubMed: 93086]

Brinkmann V, Davis MD, Heise CE, Albert R, Cottens S, Hof R, Bruns C, Prieschl E, Baumruker T, Hiestand P, et al. The immune modulator FTY720 targets sphingosine 1-phosphate receptors. J. Biol. Chem. 2002; 277:21453–21457. [PubMed: 11967257]

Brubaker RR, Beesley ED, Surgalla MJ. *Pasteurella pestis*: Role of Pesticin I and iron in experimental plague. Science. 1965; 149:422–424. [PubMed: 17809405]

Butler T. *Yersinia* infections: centennial of the discovery of the plague bacillus. Clin. Infect. Dis. 1994; 19:655–661. quiz 662–663. [PubMed: 7803628]

Cavanaugh DC, Randall R. The role of multiplication of *Pasteurella pestis* in mononuclear phagocytes in the pathogenesis of flea-borne plague. J. Immunol. 1959; 83:348–363. [PubMed: 13808585]

Charo IF, Ransohoff RM. The many roles of chemokines and chemokine receptors in inflammation. N. Engl. J. Med. 2006; 354:610–621. [PubMed: 16467548]

Cross AK, Richardson V, Ali SA, Palmer I, Taub DD, Rees RC. Migration responses of human monocytic cell lines to alpha- and beta-chemokines. Cytokine. 1997; 9:521–528. [PubMed: 9237815]

De Martini JC, Fiscus SA, Pearson LD. Macrophages in efferent lymph of sheep and their role in lectin-induced lymphocyte blastogenesis. Int. Arch. Allergy Appl. Immunol. 1983; 72:110–115. [PubMed: 6874104]

Finegold MJ. Pneumonic plague in monkeys. An electron microscopic study. Am. J. Pathol. 1969; 54:167–185. [PubMed: 4974722]

Förster R, Schubel A, Breitfeld D, Kremmer E, Renner-Müller I, Wolf E, Lipp M. CCR7 coordinates the primary immune response by establishing functional microenvironments in secondary lymphoid organs. Cell. 1999; 99:23–33. [PubMed: 10520991]

Geissmann F, Jung S, Littman DR. Blood monocytes consist of two principal subsets with distinct migratory properties. Immunity. 2003; 19:71–82. [PubMed: 12871640]

Gollmann G, Neuwirt H, Tripp CH, Mueller H, Konwalinka G, Heufler C, Romani N, Tiefenthaler M. Sphingosine-1-phosphate receptor type-1 agonism impairs blood dendritic cell chemotaxis and skin dendritic cell migration to lymph nodes under inflammatory conditions. Int. Immunol. 2008; 20:911–923. [PubMed: 18495625]

Hinnebusch BJ. The evolution of flea-borne transmission in *Yersinia pestis*. Curr. Issues Mol. Biol. 2005; 7:197–212. [PubMed: 16053250]

Janssen WA, Surgalla MJ. Plague bacillus: survival within host phagocytes. Science. 1969; 163:950–952. [PubMed: 5763880]

Jawetz E, Meyer KF. The behaviour of virulent and avirulent *P. pestis* in normal and immune experimental animals. J. Infect. Dis. 1944; 74:1–13.

Lamana A, Martin P, de la Fuente H, Martinez-Muñoz L, Cruz-Adalia A, Ramirez-Huesca M, Escribano C, Gollmer K, Mellado M, Stein JV, et al. CD69 modulates sphingosine-1-phosphate-induced migration of skin dendritic cells. J. Invest. Dermatol. 2011; 131:1503–1512. [PubMed: 21412255]

Lin KL, Suzuki Y, Nakano H, Ramsburg E, Gunn MD. CCR2+ monocyte-derived dendritic cells and exudate macrophages produce influenza-induced pulmonary immune pathology and mortality. J. Immunol. 2008; 180:2562–2572. [PubMed: 18250467]

Lönnbro P, Nordenfelt P, Tapper H. Isolation of bacteria-containing phagosomes by magnetic selection. BMC Cell Biol. 2008; 9:35. [PubMed: 18588680]

Marketon MM, DePaolo RW, DeBord KL, Jabri B, Schneewind O. Plague bacteria target immune cells during infection. Science. 2005; 309:1739–1741. [PubMed: 16051750]

Matloubian M, Lo CG, Cinamon G, Lesneski MJ, Xu Y, Brinkmann V, Allende ML, Proia RL, Cyster JG. Lymphocyte egress from thymus and peripheral lymphoid organs is dependent on S1P receptor 1. Nature. 2004; 427:355–360. [PubMed: 14737169]

McLachlan JB, Hart JP, Pizzo SV, Shelburne CP, Staats HF, Gunn MD, Abraham SN. Mast cell-derived tumor necrosis factor induces hypertrophy of draining lymph nodes during infection. Nat. Immunol. 2003; 4:1199–1205. [PubMed: 14595438]

Perry RD, Fetherston JD. *Yersinia pestis* – etiologic agent of plague. Clin. Microbiol. Rev. 1997; 10:35–66. [PubMed: 8993858]

Perry RD, Pendrak ML, Schuetze P. Identification and cloning of a hemin storage locus involved in the pigmentation phenotype of *Yersinia pestis* . J. Bacteriol. 1990; 172:5929–5937. [PubMed: 2211518]

Proudfoot AE. Chemokine receptors: multifaceted therapeutic targets. Nat. Rev. Immunol. 2002; 2:106–115. [PubMed: 11910892]

Pujol C, Bliska JB. Turning *Yersinia* pathogenesis outside in: subversion of macrophage function by intracellular yersiniae. Clin. Immunol. 2005; 114:216–226. [PubMed: 15721832]

Randolph GJ, Angeli V, Swartz MA. Dendritic-cell trafficking to lymph nodes through lymphatic vessels. Nat. Rev. Immunol. 2005; 5:617–628. [PubMed: 16056255]

Rathinasamy A, Czeloth N, Pabst O, Förster R, Bernhardt G. The origin and maturity of dendritic cells determine the pattern of sphingosine 1-phosphate receptors expressed and required for efficient migration. J. Immunol. 2010; 185:4072–4081. [PubMed: 20826749]

Rivera J, Proia RL, Olivera A. The alliance of sphingosine-1-phosphate and its receptors in immunity. Nat. Rev. Immunol. 2008; 8:753–763. [PubMed: 18787560]

Rosen H, Goetzl EJ. Sphingosine 1-phosphate and its receptors: an autocrine and paracrine network. Nat. Rev. Immunol. 2005; 5:560–570. [PubMed: 15999095]

Saikh KU, Kissner TL, Sultana A, Ruthel G, Ulrich RG. Human monocytes infected with *Yersinia pestis* express cell surface TLR9 and differentiate into dendritic cells. J. Immunol. 2004; 173:7426–7434. [PubMed: 15585868]

Sainte-Marie G, Peng FS. Structural and cell population changes in the lymph nodes of the athymic nude mouse. Lab. Invest. 1983; 49:420–429. [PubMed: 6604838]

Sebbane F, Gardner D, Long D, Gowen BB, Hinnebusch BJ. Kinetics of disease progression and host response in a rat model of bubonic plague. Am. J. Pathol. 2005; 166:1427–1439. [PubMed: 15855643]

Sebbane F, Jarrett CO, Gardner D, Long D, Hinnebusch BJ. Role of the *Yersinia pestis* plasminogen activator in the incidence of distinct septicemic and bubonic forms of flea-borne plague. Proc. Natl. Acad. Sci. USA. 2006a; 103:5526–5530. [PubMed: 16567636]

Sebbane F, Lemaître N, Sturdevant DE, Rebeil R, Virtaneva K, Porcella SF, Hinnebusch BJ. Adaptive response of *Yersinia pestis* to extracellular effectors of innate immunity during bubonic plague. Proc. Natl. Acad. Sci. USA. 2006b; 103:11766–11771. [PubMed: 16864791]

Shelburne CP, Nakano H, St John AL, Chan C, McLachlan JB, Gunn MD, Staats HF, Abraham SN. Mast cells augment adaptive immunity by orchestrating dendritic cell trafficking through infected tissues. Cell Host Microbe. 2009; 6:331–342. [PubMed: 19837373]

Shi C, Pamer EG. Monocyte recruitment during infection and inflammation. Nat. Rev. Immunol. 2011; 11:762–774. [PubMed: 21984070]

St John AL, Abraham SN. Salmonella disrupts lymph node architecture by TLR4-mediated suppression of homeostatic chemokines. Nat. Med. 2009; 15:1259–1265. [PubMed: 19855398]

Straley SC, Harmon PA. *Yersinia pestis* grows within phagolysosomes in mouse peritoneal macrophages. Infect. Immun. 1984; 45:655–659. [PubMed: 6469352]

Takabe K, Paugh SW, Milstien S, Spiegel S. "Inside-out" signaling of sphingosine-1-phosphate: therapeutic targets. Pharmacol. Rev. 2008; 60:181–195. [PubMed: 18552276]

Tsou CL, Peters W, Si Y, Slaymaker S, Aslanian AM, Weisberg SP, Mack M, Charo IF. Critical roles for CCR2 and MCP-3 in monocyte mobilization from bone marrow and recruitment to inflammatory sites. J. Clin. Invest. 2007; 117:902–909. [PubMed: 17364026]

Turner JK, McAllister MM, Xu JL, Tapping RI. The resistance of BALB/cJ mice to *Yersinia pestis* maps to the major histocompatibility complex of chromosome 17. Infect. Immun. 2008; 76:4092–4099. [PubMed: 18573896]

Une T, Brubaker RR. In vivo comparison of avirulent Vwa- and Pgm- or Pstr phenotypes of yersiniae. Infect. Immun. 1984; 43:895–900. [PubMed: 6365786]

Yona S, Kim KW, Wolf Y, Mildner A, Varol D, Breker M, Strauss-Ayali D, Viukov S, Guilliams M, Misharin A, et al. Fate mapping reveals origins and dynamics of monocytes and tissue macrophages under homeostasis. Immunity. 2013; 38:79–91. [PubMed: 23273845]

Zhang SS, Park CG, Zhang P, Bartra SS, Plano GV, Klena JD, Skurnik M, Hinnebusch BJ, Chen T. Plasminogen activator Pla of *Yersinia pestis* utilizes murine DEC-205 (CD205) as a receptor to promote dissemination. J. Biol. Chem. 2008; 283:31511–31521. [PubMed: 18650418]

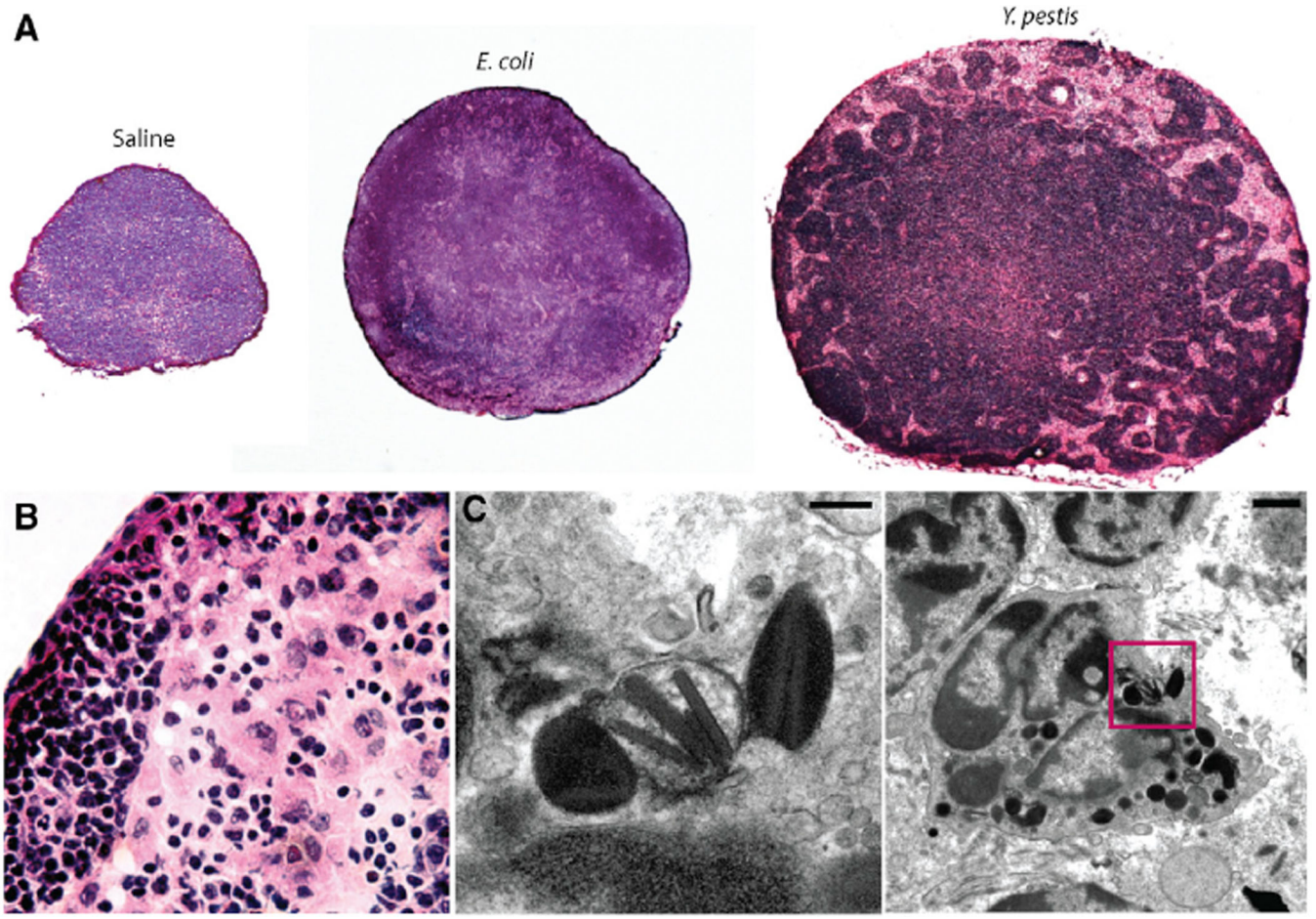

Figure 1. Buboes Contain Intracellular *Y. pestis*

(A) H&E-stained LN sections, 24 hr after injection of saline or 1×10^5 CFU of the designated bacteria, illustrate the distinction between a normal hypertrophic LN (*E. coli*) and the early stages of a bubo (*Y. pestis*). Image was obtained at 10× magnification.

(B) A LN sinus from the medullary region of an H&E-stained LN, 24 hr after infection of *Y. pestis* (40× magnification).

(C) Intracellular rod-shaped bacilli are visible within a LN (left), imaged by TEM, 72 hr after *Y. pestis* injection in the footpad. The right panel is a lower magnification of this area demonstrating that the infected cell is morphologically consistent with a macrophage. Images are representative of ≥2 independent experiments.

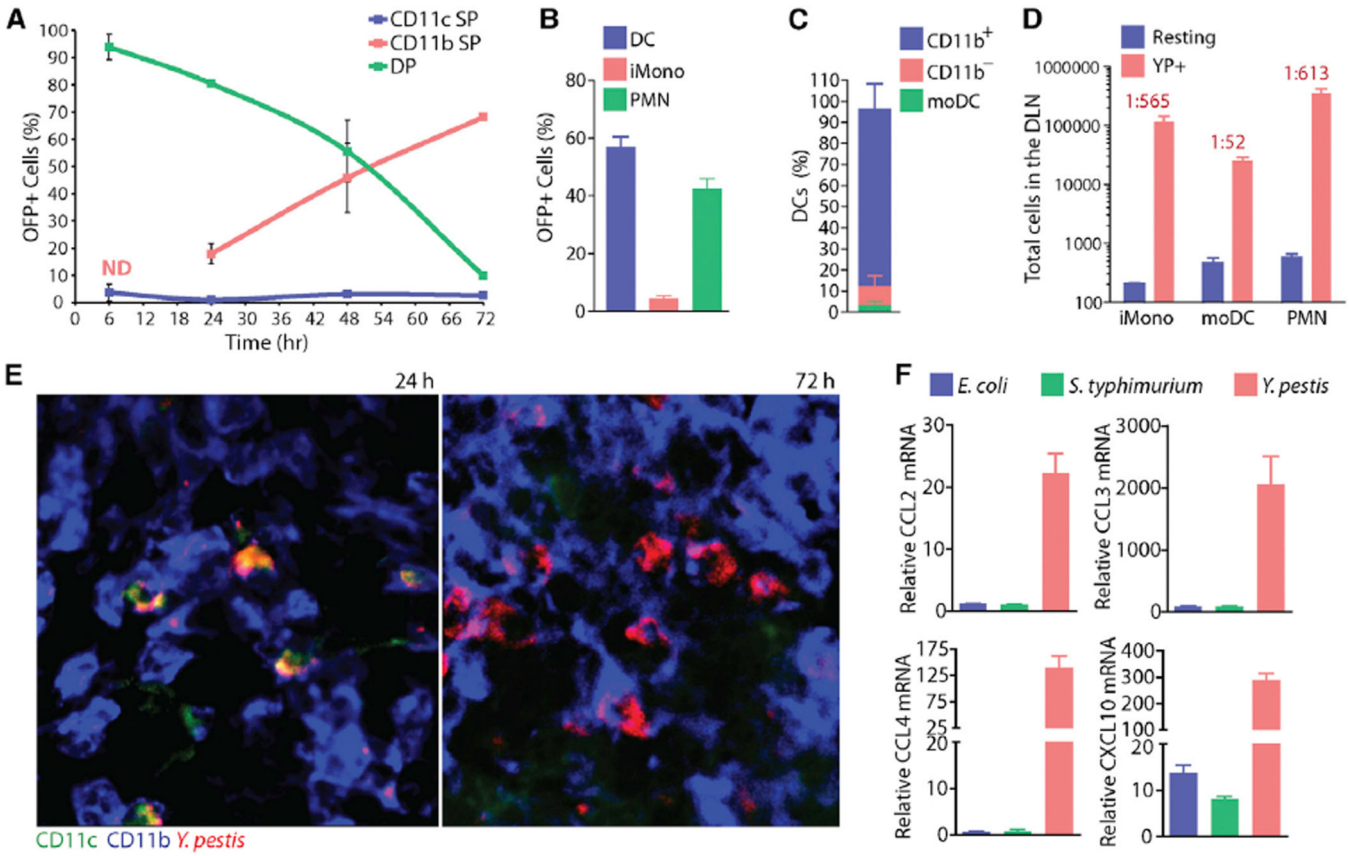

Figure 2. Two Waves of Infected Cellular Compartments within dLNs

(A) The relative phenotype of infected cells within dLNs based on staining for surface markers CD11c and CD11b as a percentage of total infected cells, determined by flow cytometry using YP-OFP to detect infected cells (n ≥ 3). Populations of single-positive (SP) and double-positive (DP) cells for each marker are presented. Abbreviation: ND, not detected. For corresponding total cell numbers see Figure S2A.

(B) Percentages of YP-OFP$^+$ cells according to phenotype 24 hr after infection after footpad infection with 5×10^5 YP-OFP. n = 5; data are representative of two independent experiments.

(C) Subsets of infected DCs (OFP$^+$CD11c$^+$IA/IE$^+$) defined by flow cytometry as a percentage of total infected DCs.

(D) The total numbers of iMono, moDC, and PMNs in either YP-OFP-infected or resting LNs were determined by flow cytometry at 24 hr. Data are representative of two independent experiments with n = 5. The ratio of each cell type is presented above the corresponding bars: resting:infected.

for (B)–(D), gating strategies are included as in Figures S2C and S2D.

(E) LN sections at 24 and 72 hr show a shift in the phenotype of the predominately infected cell (containing YP-OFP, red) from CD11c$^+$ (green) to CD11c$^-$. In both images at least some infected cells appear to be CD11b$^+$ (blue). All images are representative of three or more independent experiments with n ≥ 3. Colocalization images are provided in Figure S2E.

(F) Real-time PCR was performed to quantify mRNA levels for the chemokines CCL2, CCL3, CCL4, and CXCL10 present in LNs infected with *E. coli*, *S.* Typhimurium, or *Y. pestis*. Data are representative of three independent experiments performed with RNA from individual LNs at each time point. For a time course of chemokine production in dLNs, see Figure S2E.

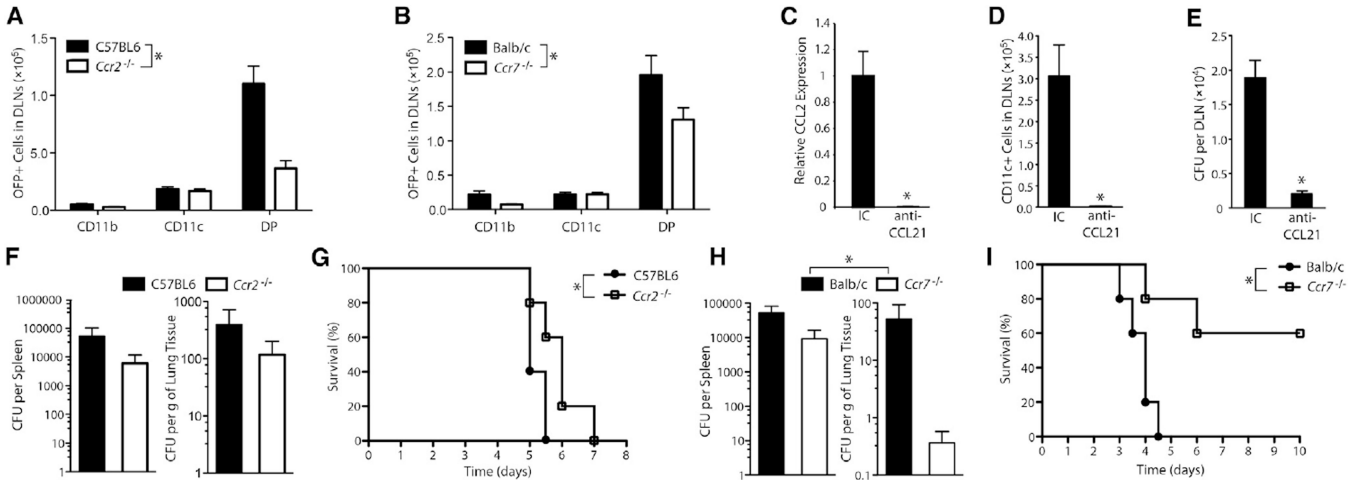

Figure 3. CCR7- and CCR2-Directed Migration Enhance *Y. pestis* Virulence In Vivo

(A and B) Graph represents the total numbers of *Y. pestis*-infected cells (OFP^+) within popliteal DLNs at 24 hr after infection with (A) $Ccr2^{-/-}$ mice and C57BL/6 controls or (B) $Ccr7^{-/-}$ mice and BALB/c controls. The cell counts for OFP^+ subsets that were single or double positive for surface markers CD11c and CD11b were determined by flow cytometry. $p < 0.0001$ by two-way ANOVA.

(C) Relative CCL2 expression in dLNs, 24 hr after infection of C57BL/6 mice with *Y. pestis*. Mice were administered an anti-CCL21 or isotype control (IC) antibody treatment 12 hr prior to infection. Real-time PCR data are representative of three independent experiments using RNA isolated from single LNs; $p < 0.05$ by Student's t test.

(D) Total numbers of $CD11c^+$ cells in the dLNs of mice were determined by flow cytometry, 24 hr after *Y. pestis* infection and with pretreatment with either IC or anti-CCL21 blocking antibody. Pretreatment with anti-CCL21 reduced the numbers of $CD11c^+$ cells in dLNs; $p < 0.05$ by Student's t test with $n = 3$.

(E) Significantly reduced CFUs were recovered from dLNs after pretreatment with anti-CCL21 blocking antibody compared to IC pretreatment, determined by Student's t test ($p = 0.0006$, $n = 4$).

(F) CFU data obtained day 3 after infection by isolating, homogenizing, and plating *Y. pestis* from spleen (left) or lung (right) tissue from $Ccr2^{-/-}$ or C57BL/6 control mice. Differences are not significant by ANOVA ($p = 0.35$); $n = 6$, pooled from two independent experiments. ND indicates not detected.

(G) Survival of $Ccr2^{-/-}$ and C57BL/6 mice after subcutaneous infection with *Y. pestis* ($n = 9–10$, pooled from two independent experiments). $Ccr2^{-/-}$ mice survived significantly longer; $p = 0.009$.

(H) CFU data for the spleen (left) and lung (right) for $Ccr7^{-/-}$ mice and BALB/c controls. Differences are not significant by ANOVA ($p = 0.06$); $n = 6–7$, pooled from two independent experiments.

(I) Survival of $Ccr7^{-/-}$ and Balb/c mice after subcutaneous infection with *Y. pestis* ($n = 5–10$, pooled from 2 independent experiments). $Ccr7^{-/-}$ mice survived significantly longer; $p = 0.0002$. For all infections in this Figure, 1×10^5 CFU of *Y. pestis* were injected in footpads

for *Ccr2*$^{-/-}$ and C57BL/6 mice and 1 × 10^7CFU of *Y. pestis* were injected for *Ccr7*$^{-/-}$ and Balb/c mice.

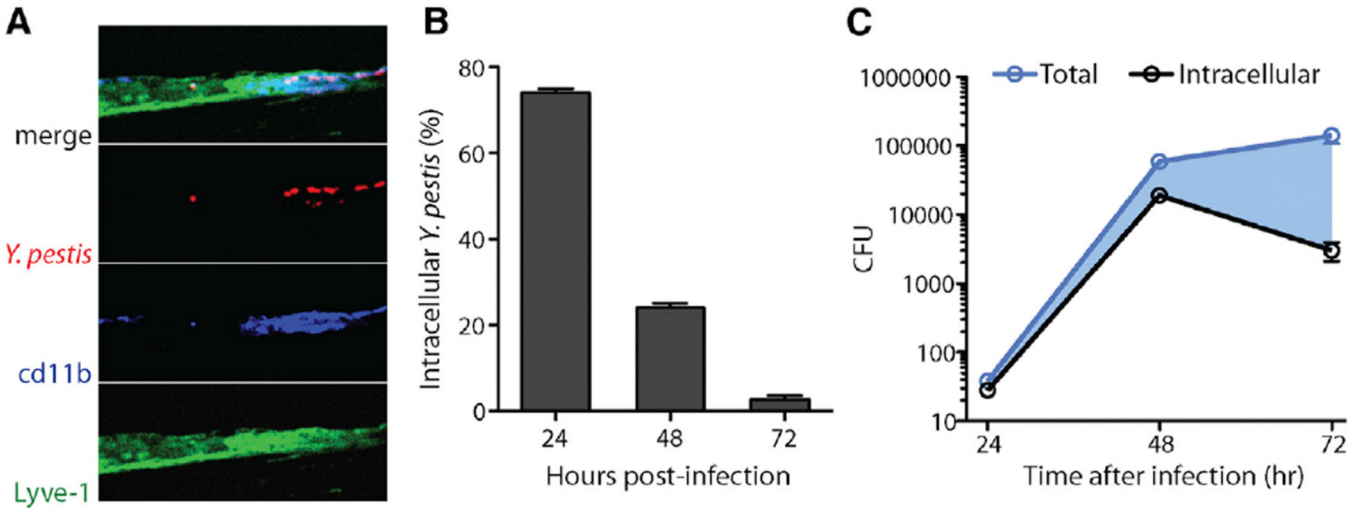

Figure 4. Intracellular *Y. pestis* Travel within Lymphatics between LNs

(A) Merged and channel series staining of mouse thigh tissue to show post-popliteal nodal lymphatic vessels (Lyve-1, green), monocytes (CD11b, blue), and OFP^+ *Y. pestis* (red). Colocalization reveals that some, but not all, $CD11b^+$ cells traveling in the postnodal lymphatics appear to contain *Y. pestis*. Images are representative of observations from two independent experiments with two mice per group.

(B) Graph represents the percentage of *Y. pestis* within the iliac node that are intracellular after footpad infection with 1×10^5 CFU. Values were obtained using a gentamicin protection assay, where a portion of the LN homogenate was treated with gentamicin to kill only the extracellular bacteria followed by washing and treatment to lyse cells. The surviving intracellular fraction was plated to determine the CFU, which is represented as a percentage of the total CFU for the organ.

(C) Graph of total and intracellular *Y. pestis*, corresponding to (B). Blue shading illustrates the growth in numbers of extracellular bacteria over time by highlighting the difference between total and intracellular bacterial counts. Data are representative of two independent experiments with n = 3–5 animals per group.

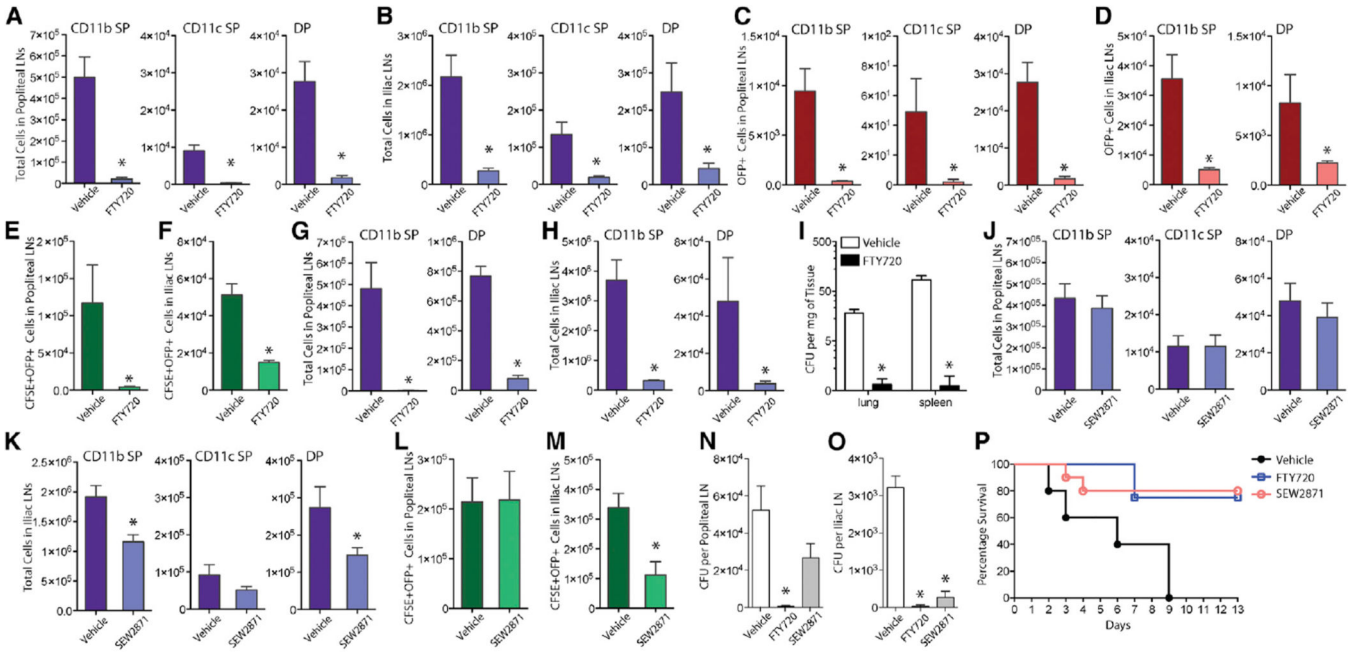

Figure 5. S1P Promotes *Y. pestis* Dissemination through Lymphoid Tissue

Animals were pretreated 24 hr before infection and then administered a daily regimen of S1P-agonist FTY720 or vehicle.

(A and B) Graphs represent the total numbers of cells staining single- (SP) and double-positive (DP) for markers CD11b and CD11c in the dLN, the popliteal LN(A) or in iliac LNs distal to dLNs (B) 24 hr after infection with *Y. pestis*.

(C and D) Graphs represent the number of cells infected by *Y. pestis* in the popliteal (C) and iliac (D) LNs, after gating on the OFP^+ population. Infected $CD11b^-$ $CD11c^+$ were not detected in iliac nodes at 24 hr.

(E and F) The graphs represent the numbers of footpad-derived cells in popliteal (E) and iliac (F) LNs that were infected with *Y. pestis*, by gating on cells $CFSE^+$ and OFP^+. CFSE labeling was performed 4 hr prior to infection with *Y. pestis* expressing OFP.

(G and H) Graphs depict numbers of $CD11b^+CD11c^{+/-}$ cells within popliteal (G) and iliac (H) LNs of mice depleted of T cells prior to infection and treatment with FTY720 or vehicle control.

(I) The CFU counts from the spleens and lungs, harvested day 3 of infection, from animals treated with FTY720 or vehicle are presented.

(J and K) Graphs represent the total number of cells with phenotypes SP or DP for CD11b and CD11c in popliteal (J) or iliac (K) LNs, 24 hr after infection and with treatment with $S1P_1$ receptor agonist SEW2871.

(L and M) Numbers of footpad-derived cells ($CFSE^+OFP^+$) in the popliteal (L) and iliac LNs (M) after SEW2871 treatment or vehicle control.

(N and O) CFUs were determined in the popliteal LN (N) and iliac LN (O), 24 hr after infection, as above.

For (A)–(H) and (J)–(M), significance was determined by Student's unpaired t test; $*p \leq 0.05$. n = 3–6 per group. For (I), significance was determined by 2-way ANOVA; $p < 0.0001$. For (N) and (O), $p < 0.05$ by 1-way ANOVA with Bonferroni's post-test.

(P) Mice were monitored for survival after infection with *Y. pestis* and treatment with FTY720, SEW2871, or vehicle control (n = 5–10 per group). Survival curves of infected mice treated with FTY720 and SEW2871 both differed significantly from the survival curve of mice treated with vehicle alone (p = 0.04 and 0.01, respectively, by log-rank test). Surviving proportions also differed significantly; p = 0.04 and 0.01, respectively, by Fisher's exact test.

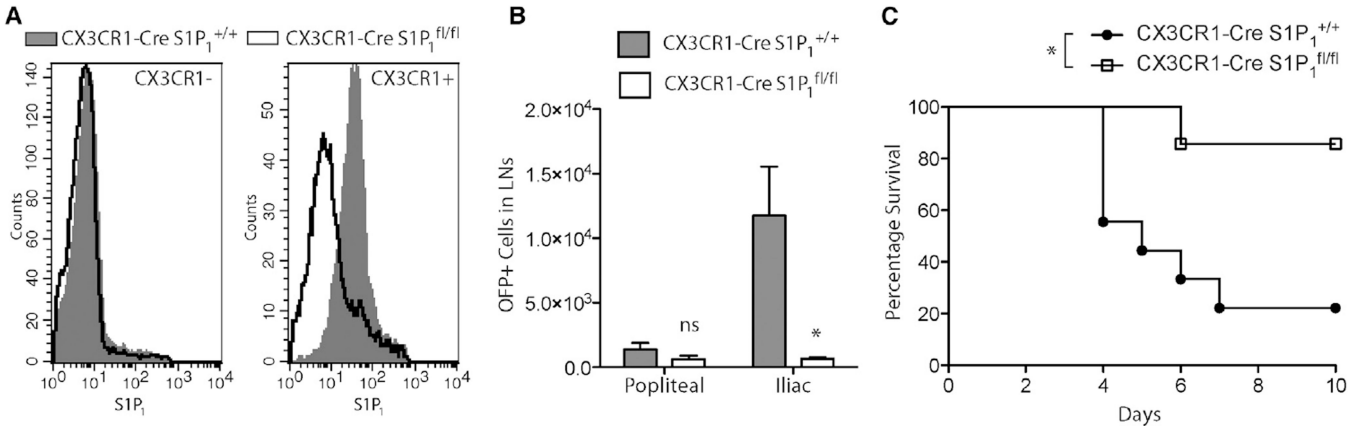

Figure 6. Conditional Deletion of $S1P_1$ in Mononuclear Phagocytes Limits Intranodal *Y. pestis* Spread

(A) S1P1 expression on CX_3CR1^+ and $CX3CR1^-$ cells in CX_3CR1-Cre $S1P_1^{fl/fl}$ mice compared to CX_3CR1-Cre $S1P_1^{+/+}$ littermate controls, determined by flow cytometry.

(B) The graphs represent the numbers of cells in popliteal and iliac LNs that were infected with *Y. pestis*, by gating on OFP^+ cells. Statistics were performed by 2-way ANOVA, where n = 4 mice per group ($p < 0.01$). Not significant = ns. Data are representative of two independent experiments.

(C) Survival of CX_3CR1-Cre $S1P_1^{fl/fl}$ and CX_3CR1-Cre $S1P_1^{+/+}$ littermate controls (n = 7–9) after footpad infection with 1×10^5 CFU of *Y. pestis*; p = 0.01 by log-rank test.